Dynamics and Mechanism of Bromate Oscillators with 1,4-Cyclohexanedione

István Szalai,[†] Krisztina Kurin-Csörgei,[†] Irving R. Epstein,*[,‡] and Miklós Orbán*[,†]

Department of Inorganic and Analytical Chemistry, L. Eötvös University, P.O. Box 32, H-1518 Budapest 112, Hungary, and Department of Chemistry, MS 015, Brandeis University, Waltham, Massachusetts 02454-9110

Received: July 15, 2003; In Final Form: September 16, 2003

Experimental and numerical studies of the temporal behavior of the acidic bromate−1,4-cyclohexanedione batch reaction in the presence of $Ce(SO_4)_2$, $MnSO_4$, or $Ru(bipy)_3SO_4$ catalyst are reported. With increasing concentration of catalyst and at $[H_2SO_4] \leq 1$ mol/dm^3 these systems show the following bifurcation sequences: uncatalyzed oscillations → clock reaction (with excitability) → catalyzed oscillations, while at $[H_2SO_4] \geq 1.5$ mol/dm^3 the sequence is uncatalyzed oscillations → catalyzed oscillations. A chemical mechanism based on kinetic measurements of some component reactions is suggested and used to simulate the experimentally found bifurcation sequences and the monotonic and nonmonotonic recovery of the system after perturbation of the excitable state. A reduced model for the bromate−CHD−catalyst system is developed and analyzed.

Introduction

The bromate−1,4-cyclohexanedione (CHD)−ferroin batch system[1] has become a frequently used tool for studying chemical waves[2−5] due to its bubble-free and long-lived oscillatory behavior. The replacement of malonic acid, the organic substrate of the classical Belousov−Zhabotinsky (BZ) reaction, by CHD not only eliminates the formation of carbon dioxide that disturbs the pattern evolution, but also generates wave dynamics significantly different from that observed in the BZ system. For example, stacked wave fronts, resulting in densely packed patterns, well segregated clusters, traveling shock structures, and merging of waves, were observed experimentally in an excitable bromate−CHD−ferroin system.[6−9] These novel modes of wave dynamics were attributed to the anomalous dispersion of the medium. Recently, stacked structures were also found in the BZ reaction when it was carried out in a reverse microemulsion,[10] where this behavior was attributed to the wave instability.[11,12] Huh and co-workers[13] described two sets of spontaneous waves separated by a long time lag in the bromate−CHD−ferroin reaction.

The chemistry of the bromate−CHD−catalyst system is much less well understood than that of the BZ reaction, which has hindered efforts to understand the peculiar behaviors observed in the former system and been an obstacle to further application of this reaction to the study of nonlinear chemical phenomena. The aim of this work is to reveal, at least partly, the mechanism of the bromate−CHD−catalyst oscillators.

The first observation of oscillations during the uncatalyzed reaction between bromate and CHD was reported by Farage and Janjic.[14] These authors studied the influence of acid concentration, oxygen, stirring, and added BZ catalysts on the oscillations, but they did not consider the mechanism of the reaction. In recent papers we have examined the chemistry of the uncatalyzed bromate−CHD−acid oscillator and have suggested a mechanism in which the experimentally identified intermediate 1,4-hydroquinone (H_2Q) plays a key role.[15,16] During the overall reaction between bromate and CHD, H_2Q is produced at a constant rate from BrCHD (the bromo derivative of CHD) and is oxidized autocatalytically to 1,4-benzoquinone (Q). The time scale separation between the slow production and the fast autocatalytic consumption of H_2Q leads to the oscillatory kinetics. A recent NMR study by Britton[17] provides additional support for this mechanism.

To exploit the advantages offered by the bromate−CHD system for studying temporal and spatial dynamics, an indicator is added to make visible any oscillations or pattern formation that occur. For the purpose of visualization, many redox indicators, including the BZ catalysts ferroin and $Ru(bipy)_3SO_4$, can be used.[18] However, the presence of a BZ catalyst may change the kinetics and dynamics of the bromate−CHD system and the "uncatalyzed" oscillations can turn into a "BZ-type" version, if the concentration of the catalyst exceeds a threshold ($\sim 10^{-4}$ mol/dm^3).

We recently developed a chemical model for the bromate−CHD−ferroin oscillator by extending the mechanism of the bromate−CHD system with steps involving the reactions of ferroin and ferriin.[19] This extended version contains two competitive autocatalytic pathways: in the first H_2Q and in the second ferroin serves as the reductant. The ferriin produced in the autocatalytic cycle can be reduced back to ferroin in several ways: it oxidizes CHD to the end product Q via H_2Q; it reacts with BrCHD to form Q and the intermediate Br^-; and it oxidizes H_2Q to Q (see Figure 5).

In this paper we continue our mechanistic work on the bromate−CHD−catalyst (Ce(IV), Mn(II), and $Ru(bipy)_3^{2+}$) oscillators. The presence of these catalysts in the bromate−CHD oscillator allows the experimentalist to apply a variety of techniques, including visible spectrometry, NMR,[17] or ESR, to follow the evolution of the system or its response to perturbation, which cannot be done in the absence of such indicator species. Kinetic data for some of the component reactions in our model, the model itself, and simulations of oscillations and excitability in the catalyzed systems are presented.

Experimental Section

H_2SO_4 (Chemolab 96%), 1,4-cyclohexanedione (Aldrich 98%), KBr (Reanal p.a.), $NaBrO_3$ (Fluka p.a.), $MnSO_4 \cdot H_2O$,

[†] L. Eötvös University.
[‡] Brandeis University.

10.1021/jp0360523 CCC: $25.00
Published on Web 10/31/2003

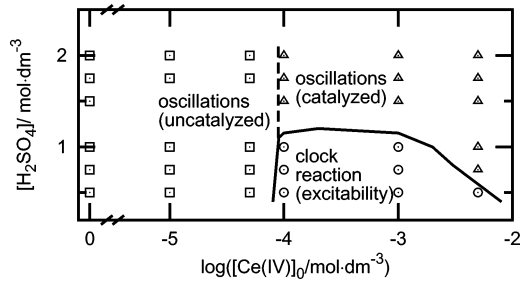

Figure 1. Experimental bifurcation diagram of transient dynamic behavior in the 1,4-cyclohexanedione−bromate−Ce(IV) system. Experimental conditions: [CHD] = 0.1 mol/dm^3; [BrO_3^-] = 0.1 mol/dm^3; T = 20 °C.

$Ce(NH_4)_4(SO_4)_4 \cdot 2H_2O$ (Reanal), $Ru(bipy)_3Cl_2 \cdot 6H_2O$ (Aldrich), and bidistilled water were used to prepare the working solutions. Stock solutions of 0.025 mol/dm^3 ferroin were prepared from $FeSO_4 \cdot 7H_2O$ (Reanal p.a.) and 1,10-phenantroline (Aldrich 99%).

$Ru(bipy)_3SO_4$ was obtained by converting the chloride salt to sulfato form using the recipe of Gao and Försterling.[21] Stock solutions of $Ru(bipy)_3^{3+}$ were prepared from stock solutions of $Ru(bipy)_3^{2+}$ by oxidation with solid PbO_2 followed by filtration. Because of their instability, the solutions were stored in darkness and used within 1 h. $Mn_2(SO_4)_3$ stock solution was prepared by reacting a known amount of $KMnO_4$ with a 50-fold excess of $MnSO_4$ in 2 mol/dm^3 of sulfuric acid.

The bromo derivative of CHD was prepared by mixing CHD with a stoichiometric amount of bromine. The reaction is regarded to be complete when the bromine color disappears. This process is relatively slow, so the decomposition of BrCHD according to eqs R9 and R10 is taken into account when the initial concentration of BrCHD is calculated.

Spectra for the kinetic measurements were taken on Milton Roy 3000 and Agilent 8452 diode array spectrophotometers equipped with quartz cells (path length 1 cm, volume 2 mL). Redox potentials were monitored with a smooth Pt electrode (Radelkis) and a $Hg/Hg_2SO_4/K_2SO_4$(sat.) reference electrode (Radiometer). Analog signals were digitized with a 12 bit AD converter (Labtech PCL-711 S) and processed on a PC. The temperature was kept at 20.0(±0.1) °C, and the solutions in the cell were mixed with a magnetic stirrer.

The simulations were done with the program LSODE.[22] The parameter estimations were carried out with the MULTIMRQ program, which uses the Marquardt method. Fitted parameters are given at 95% significance level.

Results and Discussion

Temporal Dynamics in Batch Reactor. The dynamics of the acidic bromate−CHD−catalyst systems (catalyst = Ce(IV), Mn(II), $Ru(bipy)_3SO_4$, ferroin) was studied under batch conditions, and the concentrations of sulfuric acid and the catalyst were varied. The initial concentrations of CHD and bromate were kept constant at 0.1 mol/dm^3. A phase diagram summarizing the transient dynamical behaviors observed for the cerium-catalyzed system is shown in Figure 1. Bifurcation diagrams for the other catalysts are similar.

In Figure 1 we encounter three types of behavior as the catalyst concentration is increased: two kinds of oscillations and a clock reaction. The first type of oscillations, which appear at zero or low concentration of the catalyst, are driven by the formation and consumption of H_2Q and are referred to as "uncatalyzed" oscillations, because the catalyst here acts mainly as an indicator of the oscillations. The catalyst appears to hinder

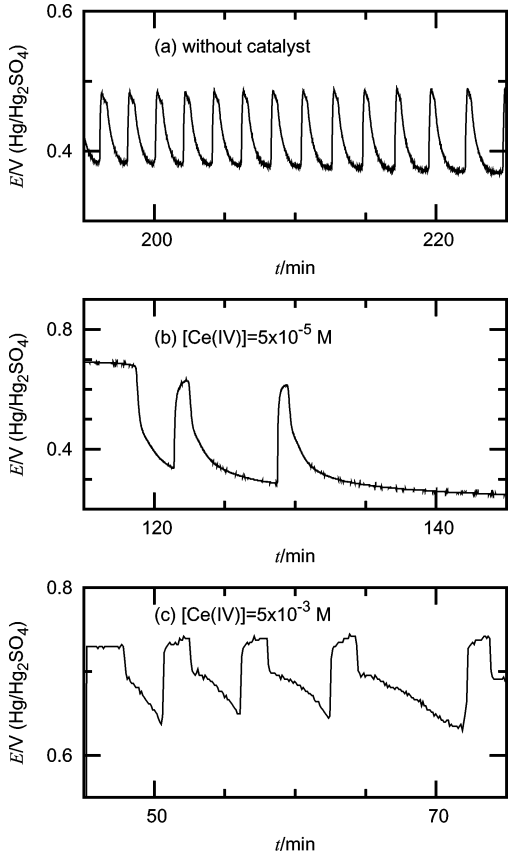

Figure 2. Effect of cerium(IV) on the 1,4-cyclohexanedione−bromate−sulfuric acid system. Experimental conditions: [H_2SO_4] = 1.0 mol/dm^3; [CHD] = 0.1 mol/dm^3; [BrO_3^-] = 0.1 mol/dm^3; (a) without catalyst; (b) [Ce(IV)] = 5.0×10^{-5} mol/dm^3; (c) [Ce(IV)] = 5.0×10^{-3} mol/dm^3; T = 20 °C.

the H_2Q-regulated oscillations; as the catalyst concentration is increased, the oscillations become slower and fewer in number. When its concentration exceeds a critical value the "uncatalyzed" oscillations are either replaced by a clock reaction or start to show the features of the "catalyzed" oscillations.

The clock reaction behavior appears at low acid concentration ([H_2SO_4] ≤ 1 mol/dm^3). When the acid concentration is high ([H_2SO_4] ≥ 1.5 mol/dm^3) the system still oscillates but some characteristics of the oscillations change proportionally with the catalyst concentration; the shape of the oscillatory traces is modified (the system stays in the oxidized state for much longer), the number of oscillations significantly decreases, the period increases, and the potential range of the oscillations shifts to higher values. The oscillations that appear above the threshold catalyst concentration are referred to as "catalyzed" or "BZ-type". The catalyst concentration above which clock reaction or the "catalyzed" oscillations take place is approximately 10^{-4} mol/dm^3 for ferroin, 8×10^{-5} mol/dm^3 for Ce(IV) and Mn(II), and 5×10^{-6} mol/dm^3 for $Ru(bipy)_3SO_4$. Note that these concentration limits are inversely related to the rates of reaction between CHD and the oxidized form of the catalyst (see below).

Figures 2 and 3a depict the effect of Ce(IV) concentration. The oscillations measured in the catalyst-free system are seen in Figure 2a. On increasing the catalyst concentration, the number of oscillations decreases and the period increases (Figure 2b). Above a threshold value of [Ce(IV)], the clock reaction takes place (Figure 3a). At a second threshold "catalyzed" oscillations, shown in Figure 2c, appear. In Figure 4 the effect of Mn(II) and $Ru(bipy)_3^{2+}$ on the catalyst-free bromate−CHD system is presented.

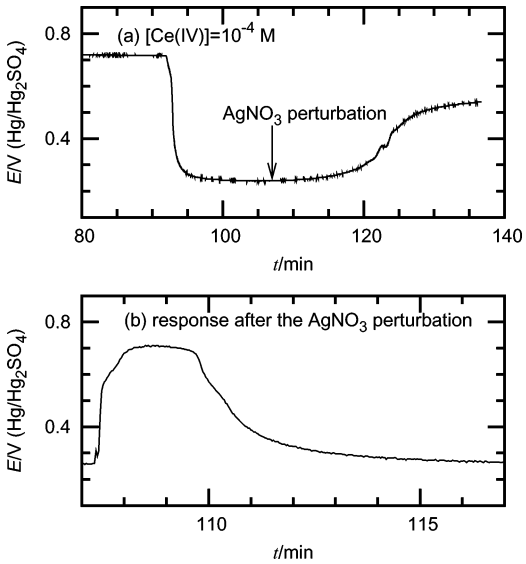

Figure 3. Clock reaction (a) and excitability (b) in the 1,4-cyclohexanedione−bromate−cerium(IV) system. Experimental conditions: $[H_2SO_4] = 1.0$ mol/dm^3; [CHD] = 0.1 mol/dm^3; $[BrO_3^-] = 0.1$ mol/dm^3; [Ce(IV)] = 1.0×10^{-4} mol/dm^3. In part (b), perturbation of the clock reaction with $[AgNO_3] = 1.5 \times 10^{-4}$ mol/dm^3 is made at the time indicated by the arrow in part (a). $T = 20$ °C.

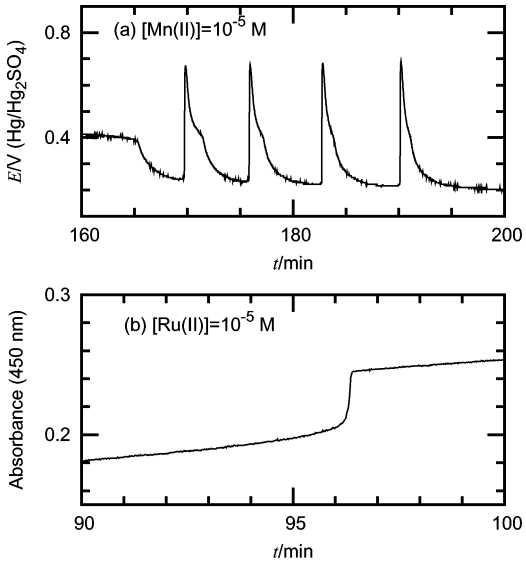

Figure 4. Effect of Mn(II) and $[Ru(bipy)_3]^{2+}$ on the 1,4-cyclohexanedione−bromate−sulfuric acid system. Experimental conditions: $[H_2SO_4] = 1.0$ mol/dm^3; [CHD] = 0.1 mol/dm^3; $[BrO_3^-] = 0.1$ mol/dm^3; (a) [Mn(II)] = 1.0×10^{-5} mol/dm^3; (b) [Ru(II)] = 1.0×10^{-5} mol/dm^3; $T = 20$ °C.

In the "clock reaction" region the system switches suddenly from the oxidized state to an excitable reduced state and stays there for a relatively long time before it switches back to the oxidized state with a slow sigmoidal transition. The excitability in the reduced state was demonstrated by perturbing the system with small amounts of $AgNO_3$ or $Hg(NO_3)_2$. The response of the system to a superthreshold perturbation with $AgNO_3$ is shown in Figure 3b.

Kinetics of the Organic Subset in the Mechanism. *The Organic Subset during the Oxidation of CHD by Bromate and by the Oxidized Form of the Catalyst.* The oxidation of CHD proceeds through several intermediates to quinone. The most important species that we propose in the overall process are shown in Figure 5.

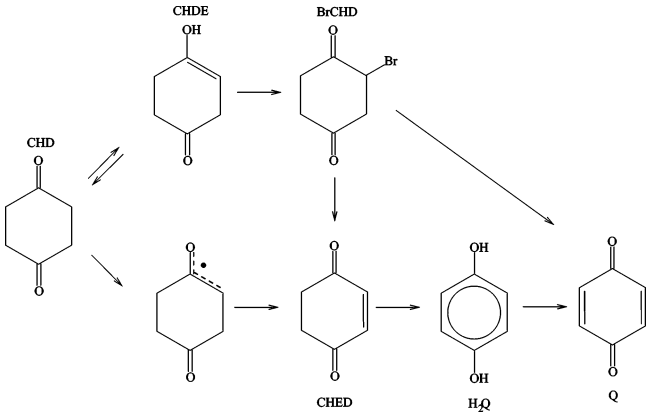

Figure 5. Key organic species in the oxidation of 1,4-cyclohexanedione by bromate (upper pathway) and by catalyst (lower pathway). Abbreviations: CHD, 1,4-cyclohexanedione; CHDE, enol form of CHD; BrCHD, 2-bromo-1,4-cyclohexanedione; CHED, 2-cyclohexene-1,4-dione; H_2Q, 1,4-hydroquinone; Q, 1,4-benzoquinone.

Oxidation of CHD and BrCHD. The rate of the oxidation of CHD and BrCHD by Ce(IV), Mn(III), and $[Ru(bipy)_3]^{3+}$ was measured by following the change in absorbance at $\lambda = 330$, 450, and 480 nm (characteristic for the absorption of Ce(IV), $[Ru(bipy)_3]^{2+}$, and Mn(III), respectively).

The rate equation and the rate constant were established from experiments carried out with the following initial concentrations: CHD or BrCHD (0.01−0.1 mol/dm^3), oxidants (10^{-5}−10^{-4} mol/dm^3), and sulfuric acid (1.0 mol/dm^3). Figure 6 presents the experimentally obtained absorbance vs time curves of the oxidation of CHD and BrCHD and the fitted curves (dotted lines) for determination of the rate constants. The results are summarized in Table 1. For better comparison the table is augmented with data for oxidation by ferriin.[19] We find that with all the catalysts, the stoichiometry and kinetics are given by:

$$2Ox^{n+} + CHD \rightarrow 2Red^{(n-1)+} + H_2Q + 2H^+ \quad (R16)$$

$$v_{16} = k_{16} \times [Ox^{n+}] \times [CHD] \quad (1)$$

$$2Ox^{n+} + BrCHD \rightarrow Q + Br^- + 3H^+ + 2Red^{(n-1)+} \quad (R17)$$

$$v_{17} = k_{17} \times [Ox^{n+}] \times [BrCHD] \quad (2)$$

Oxidation of H_2Q. The oxidation of H_2Q by Ce(IV), Mn(III), and $[Ru(bipy)_3]^{3+}$ is too fast to measure with our experimental setup. These reactions are assumed to take place according to the stoichiometry and kinetics of (R18) and eq 3.

$$2Ox^{n+} + H_2Q \rightarrow 2Red^{(n-1)+} + Q + 2H^+ \quad (R18)$$

$$v_{18} = k_{18} \times [Ox^{n+}] \times [H_2Q] \quad (3)$$

The rate constant for reaction R18 was treated as an adjustable parameter in the simulations (Table 2). In our simulations we use slightly lower values of k_{18} for the oxidation of H_2Q by Mn(III) and Ce(IV) than those determined by Wells and Kuritsyn in 1 mol/dm^3 perchloric acid solution,[23] which is justified by the known formation of sulfato complexes in the 1−2.5 mol/dm^3 sulfuric acid media used in our experiments.

The Model and Simulations. *The Model.* Based on our kinetic measurements, we developed a model that consists of 30 reactions and 16 variables. The model and the corresponding rate constants are presented in Tables 3 and 4. Most of the rate

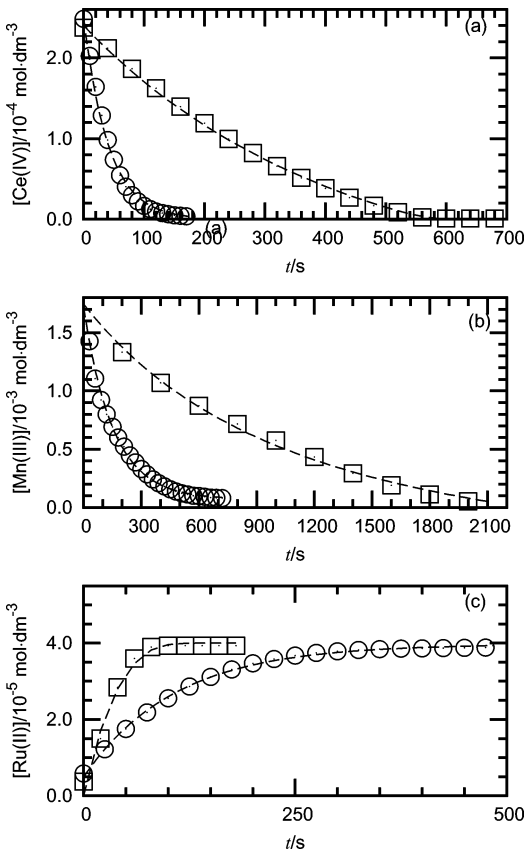

Figure 6. Oxidation of CHD and BrCHD. Experimental conditions: $[H_2SO_4] = 1.0$ mol/dm^3; $T = 20$ °C; (a) [Ce(IV)] = 2.5×10^{-4} mol/dm^3, [BrCHD] = 2.4×10^{-3} mol/dm^3 (⊡), [CHD] = 2.5×10^{-2} mol/dm^3 (⊙), $\lambda = 330$ nm, $\epsilon_{330}^{Ce(IV)} = 5500$ mol^{-1} dm^3 cm^{-1}; (b) [Mn(III)] = 1.7×10^{-3} mol/dm^3, [BrCHD] = 2.9×10^{-3} mol/dm^3 (⊡), [CHD] = 2.0×10^{-2} mol/dm^3 (⊙), $\lambda = 480$ nm, $\epsilon_{480}^{Mn(III)} = 120$ mol^{-1} dm^3 cm^{-1}; (c) [Ru(III)] = 4.0×10^{-5} mol/dm^3, [Ru(II)] = 7.0×10^{-6} mol/dm^3, [BrCHD] = 2.9×10^{-3} mol/dm^3 (⊡), [CHD] = 1.0×10^{-3} mol/dm^3 (⊙), $\lambda = 450$ nm, $\epsilon_{450}^{[Ru(bipy)_3]3+} = 150$ mol^{-1} dm^3 cm^{-1}, $\epsilon_{450}^{[Ru(bipy)_3]2+} = 14500$ mol^{-1} dm^3 cm^{-1}.

TABLE 1: Measured Rate Constants for Oxidation of CHD (k_{16}) and BrCHD (k_{17}) in 1 mol/dm^3 H_2SO_4

Ox	k_{16}, mol^{-1} dm^3 s^{-1}	k_{17}, mol^{-1} dm^3 s^{-1}	ref
$[Fe(phen)_3]^{3+}$	0.11(±0.01)	0.051(±0.001)	19
Mn(III)	0.16(±0.01)	0.19(±0.02)	this work
Ce(IV)	0.47(±0.02)	0.51(±0.02)	this work
$[Ru(bipy)_3]^{3+}$	4.60(±0.1)	4.70(±0.1)	this work

TABLE 2: Adjusted Rate Constants for Oxidation of H_2Q in 1 mol/dm^3 H_2SO_4

Ox	k_{18}, mol^{-1} dm^3 s^{-1}	ref
Ce(IV)	1×10^2	this work
Mn(III)	1×10^3	this work
$[Fe(phen)_3]^{3+}$	6×10^3	19
$[Ru(bipy)_3]^{3+}$	6×10^4	this work

constants were determined experimentally. The most important elements of the model are the following: (i) the consumption of control intermediate Br^- in steps R1−R3, (ii) the two pathways of autocatalysis [(R5a) + (R5b) + (R6a)] and [(R5a) + (R5b) + (R6b)], and (iii) the regeneration of Br^- and H_2Q, mainly in reactions R9−R10 and in R16−R17. In the model Ox^{n+} and $Red^{(n-1)+}$ represent Ce(IV), Mn(III), $Ru(bipy)_3^{3+}$ and Ce(III), Mn(II), $Ru(bipy)_3^{2+}$, respectively. The model simulates qualitatively the main features of the batch dynamics observed in the bromate−CHD systems both in the absence and in the presence of catalyst.

TABLE 3: Model of the Bromate−CHD−Redox Catalyst Oscillatory System[a]

	reactions
R1	$Br^- + HOBr + H^+ \rightleftharpoons Br_2 + H_2O$
R2	$Br^- + HBrO_2 + H^+ \rightleftharpoons 2HOBr$
R3	$Br^- + BrO_3^- + 2\,H^+ \rightleftharpoons HOBr + HBrO_2$
R4a	$HBrO_2 + H^+ \rightleftharpoons H_2BrO_2^+$
R4b	$HBrO_2 + H_2BrO_2^+ \rightarrow BrO_3^- + HOBr + 2H^+$
R5a	$HBrO_2 + BrO_3^- + H^+ \rightleftharpoons Br_2O_4 + H_2O$
R5b	$Br_2O_4 \rightleftharpoons 2BrO_2^\bullet$
R6a	$H_2Q + 2BrO_2^\bullet \rightarrow 2HBrO_2 + Q$
R6b	$Red^{(n-1)+} + BrO_2^\bullet + H^+ \rightleftharpoons Ox^{n+} + HBrO_2$
R7	$CHD + H^+ \rightleftharpoons CHDE + H^+$
R8	$CHDE + Br_2 \rightarrow BrCHD + Br^- + H^+$
R9	$BrCHD + H^+ \rightarrow CHED + Br^- + 2H^+$
R10	$CHED + H^+ \rightarrow H_2Q + H^+$
R11	$CHD + BrO_3^- + H^+ \rightarrow H_2Q + HBrO_2 + H_2O$
R12	$CHD + HBrO_2 \rightarrow H_2Q + HOBr + H_2O$
R13	$H_2Q + BrO_3^- + H^+ \rightarrow Q + HBrO_2 + H_2O$
R14	$H_2Q + HOBr \rightarrow Q + Br^- + H^+ + H_2O$
R15	$H_2Q + Br_2 \rightarrow Q + 2Br^- + 2H^+$
R16	$2Ox^{n+} + CHD \rightarrow 2Red^{(n-1)+} + H_2Q + 2H^+$
R17	$2Ox^{n+} + BrCHD \rightarrow Q + Br^- + 3H^+ + 2Red^{(n-1)+}$
R18	$2Ox^{n+} + H_2Q \rightarrow 2Red^{(n-1)+} + Q + 2H^+$
R19	$2Red^{(n-1)+} + BrO_3^- + 3H^+ \rightarrow 2Ox^{n+} + HBrO_2 + H_2O$

[a] Symbols for the organic species: CHD = 1,4-cyclohexanedione, CHDE = enol form of CHD, BrCHD = 2-bromo-1,4-cyclohexanedione, CHED = 2-cyclohexene-1,4-dione, H_2Q = 1,4-hydroquinone; Q = 1,4-benzoquinone.

TABLE 4: Rate Constants for a Model of the Bromate−CHD−Redox Catalyst Oscillatory System[a]

	$k_{forward}$	$k_{reverse}$	ref
R1	8×10^9 mol^{-2} dm^6 s^{-1}	80 s^{-1}	25
R2	2.5×10^6 mol^{-2} dm^6 s^{-1}	2×10^{-5} mol^{-1} dm^3 s^{-1}	25
R3	1.2 mol^{-3} dm^9 s^{-1}	3.2 mol^{-2} dm^6 s^{-1}	21
R4a	2×10^6 mol^{-1} dm^3 s^{-1}	1×10^8 s^{-1}	26
R4b	1.7×10^5 mol^{-1} dm^3 s^{-1}		26
R5a	48 mol^{-2} dm^6 s^{-1}	3.2×10^3 s^{-1}	21
R5b	7.5×10^4 s^{-1}	1.4×10^9 mol^{-1} dm^3 s^{-1}	21
R6a	2×10^6 mol^{-1} dm^3 s^{-1}		19
R6b			
$[Fe(phen)_3]^{2+}$	1×10^7 mol^{-2} dm^6 s^{-1}		24
$[Ru(bipy)_3]^{2+}$	4×10^6 mol^{-2} dm^6 s^{-1}		21
Ce(III)	6.2×10^4 mol^{-2} dm^6 s^{-1}	1.2×10^4 mol^{-1} dm^3 s^{-1}	21
Mn(II)	8.5×10^4 mol^{-2} dm^6 s^{-1}	7.7×10^4 mol^{-1} dm^3 s^{-1}	28
R7	2.1×10^{-4} mol^{-1} dm^3 s^{-1}	5.2×10^2 mol^{-1} dm^3 s^{-1}	15
R8	2.8×10^9 mol^{-1} dm^3 s^{-1}		15
R9	5×10^{-5} mol^{-1} dm^3 s^{-1}		15
R10	1.9×10^{-4} mol^{-1} dm^3 s^{-1}		15
R11	2×10^{-5} mol^{-2} dm^6 s^{-1}		15
R12	5 mol^{-2} dm^6 s^{-1}		19
R13	2×10^{-2} mol^{-2} dm^6 s^{-1}		19
R14	6×10^5 mol^{-1} dm^3 s^{-1}		15
R15	1×10^4 mol^{-1} dm^3 s^{-1}		19
R16, R17	see Table 1		
R18	see Table 2		
R19			
$[Fe(phen)_3]^{2+}$	0.02 mol^{-3} dm^9 s^{-1}		19

[a] The values refer to a temperature of 20 °C. $[H_2O] = 55$ mol/dm^3 is included in the rate constants. We used hydrogen ion concentrations reported by Robertson and Dunford (e.g. in 1, 2, and 3 mol/dm^3 sulfuric acid, $[H^+] = 1.29, 2.65, 3.98$, respectively).[27] This is a mass action kinetic model with the exception of $v_{6a} = k_{6a} \times [H_2Q] \times [BrO_2^\bullet]$, $v_{16} = k_{16} \times [Ox^{n+}] \times [CHD]$, $v_{17} = k_{17} \times [Ox^{n+}] \times [BrCHD]$, $v_{18} = k_{18} \times [Ox^{n+}] \times [H_2Q]$, $v_{19} = k_{19} \times [Red^{(n-1)+}] \times [BrO_3^-] \times [H^+]^2$.

The Dynamical Behavior. Reactions R1−R15 excluding step R6b describe the uncatalyzed oscillations. Steps R1−R19 are needed to account for the "BZ-type" oscillations and the clock behavior with excitability.

The main steps in the uncatalyzed oscillations, as shown in ref 15, are the slow production of H_2Q and Br^- from BrCHD

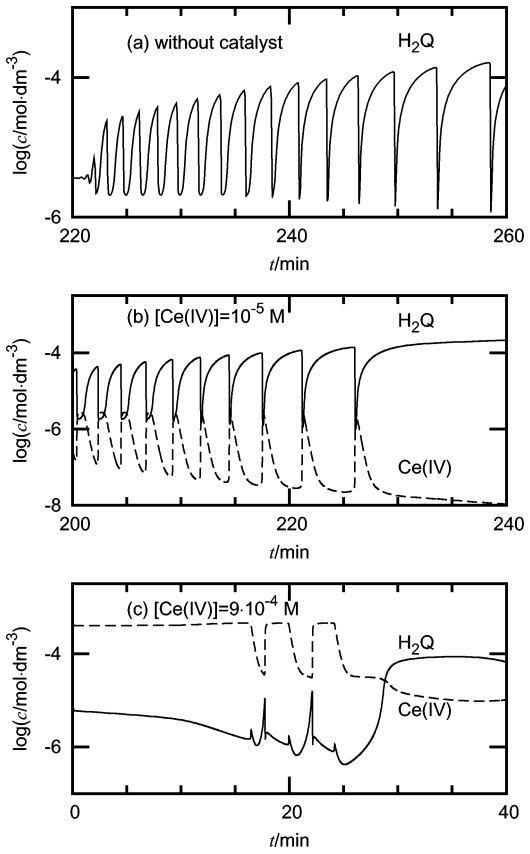

Figure 7. Simulations of the effect of Ce(IV) on the 1,4-cyclohexanedione−bromate−sulfuric acid system with the full model. Initial values: $[H_2SO_4] = 1.0$ mol/dm^3; [CHD] = 0.1 mol/dm^3; $[BrO_3^-] = 0.1$ mol/dm^3; (a) without catalyst; (b) $[Ce(IV)] = 1.0 \times 10^{-5}$ mol/dm^3; (c) $[Ce(IV)] = 9.0 \times 10^{-4}$ mol/dm^3.

in steps R9 and R10 and the autocatalytic production of $HBrO_2$ induced by H_2Q via reactions R5a−R6a. If catalyst is present, it also produces H_2Q and Br^- [(R16), (R17)] and participates in the autocatalytic formation of $HBrO_2$ in process R6b. When reactions R6b, R16, and R17 are slow (i.e., the concentration of the catalyst is zero or below the critical value) the oscillatory cycle is governed by the formation of H_2Q through (R9)−(R10), and its autocatalytic consumption via (R6a), and the system therefore functions as an uncatalyzed oscillator. These oscillations persist until the production and consumption of H_2Q are balanced. When the formation of H_2Q exceeds its consumption, the system ends up in a reduced state. Simulations of the uncatalyzed oscillations are shown in Figure 7a. Below the critical concentration of the catalyst the system shows "uncatalyzed" oscillations (Figures 7b and 8a). With increasing concentration of the catalyst reactions R16 and R17 successfully compete with reactions R9, R10, and R6a, and they produce a significant amount of H_2Q and Br^-. As a result, the uncatalyzed oscillations are suppressed and the system exhibits clock reaction behavior (Figures 8b and 9a) or the catalyzed oscillatory state at higher catalyst concentration (Figure 7c). High acidity promotes the production of bromine via steps R1 + R2 + R3:

$$5Br^- + BrO_3^- + 6H^+ \rightarrow 3Br_2 + H_2O (3 \times R1 + R2 + R3)$$

The bromine consumes H_2Q in fast reaction R15, which may explain why the domain of catalyzed oscillations increases with increasing acid concentration.

The model successfully simulates the experimental dependence of the oscillatory period on catalyst concentration,[1] which

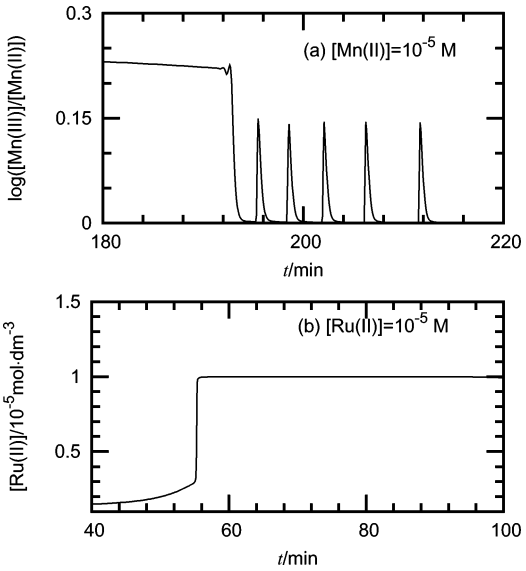

Figure 8. Simulations of the effect of Mn(II) and $[Ru(bipy)_3]^{2+}$ on the 1,4-cyclohexanedione−bromate−sulfuric acid system. Initial values: $[H_2SO_4] = 1.0$ mol/dm^3; [CHD] = 0.1 mol/dm^3; $[BrO_3^-] = 0.1$ mol/dm^3; (a) $[Mn(II)] = 1.0 \times 10^{-5}$ mol/dm^3; (b) $[Ru(II)] = 1.0 \times 10^{-5}$ mol/dm^3; $T = 20$ °C.

shows a clear break between the concentration ranges in which the system behaves like an "uncatalyzed" or a "catalyzed" oscillator.

We also simulated the experimental phase diagram that shows the transient behavior of the bromate−CHD−Ce(IV) batch reaction shown in Figure 1. The simulated phase diagram, presented in Figure 10, renders all the major domains of behavior observed in the system when the concentrations of sulfuric acid and catalyst are varied. The model can also reproduce the order of the threshold catalyst concentrations ([ferroin] < [Ce(IV)] and [Mn(II)] < $[Ru(bipy)_3^{2+}]$) above which clock reaction or the catalyzed oscillations take place.

One of the most attractive features of the bromate−CHD−catalyst oscillator is its peculiar wave dynamics. As was shown by the Steinbock group, this system with ferroin shows several types of pulse interactions, such as wave stacking, merging, and bunching.[6−8] The authors interpreted these phenomena in terms of the anomalous (nonmonotonic and nonoscillatory) dispersion of the medium. It is known that the manner of recovery after an excitation (monotonic, oscillatory, or nonmonotonic and nonoscillatory) determines the dispersion relation of the excitable system: monotonic recovery indicates normal dispersion but nonmonotonic recovery leads to an anomalous dispersion relation.[29]

We also studied numerically the excitability of the system. Because the reaction is studied under batch conditions, the states are not stationary and the excitability threshold changes during the course of the reaction. During the clock reaction the system stays in the reduced state for a certain period of time. This state is excitable, i.e., a small perturbation rapidly damps out, but a perturbation that exceeds the threshold value grows larger before the system returns to the reduced state after a long cycle (Figure 9). We found different behaviors in the excitable region of the phase diagram (Figure 10). The recovery can be monotonic for all species shown in Figure 9, but there is also a relatively large domain with nonmonotonic, nonoscillatory recovery for Br^- and monotonic recovery for H_2Q and Ce(IV) at intermediate catalyst concentrations and high acidity in the excitable region (Figure 11). The decay of the perturbed state is regarded as nonmonotonic if the concentration of a species (like Br^- in Figure 11a)

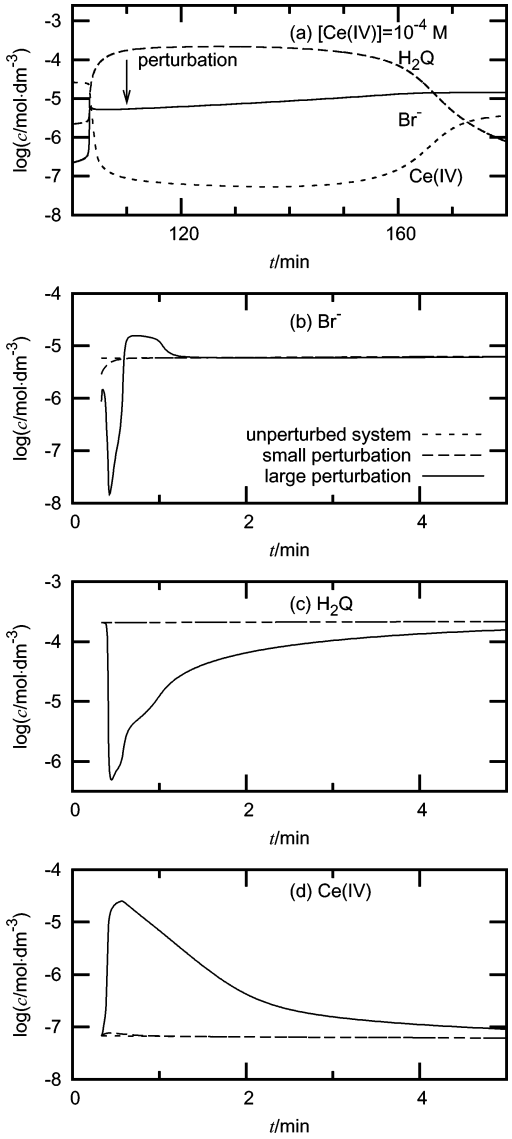

Figure 9. Simulation of clock reaction (a) and excitability (b, c, and d) at $[Ce(IV)] = 1.0 \times 10^{-4}$ mol/dm^3. Response of the system after perturbation of $[Br^-]$ (b), $[H_2Q]$ (c), and [Ce(IV)] (d). Initial values: $[H_2SO_4] = 1.0$ mol/dm^3; $[BrO_3^-] = 0.1$ mol/dm^3; [CHD] = 0.09 mol/dm^3. The arrow indicates when the perturbation was applied. $[Br^-]$ in the unperturbed system is 5.8×10^{-6} mol/dm^3. A small perturbation that decreases $[Br^-]$ (to 2.8×10^{-6} mol/dm^3) results in a smooth recovery, while a larger perturbation (to $[Br^-] = 8.6 \times 10^{-7}$ mol/dm^3) gives excitability.

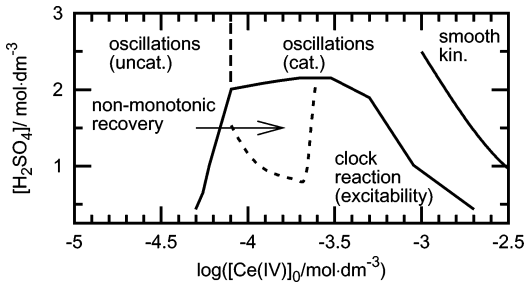

Figure 10. Simulated phase diagram of transient dynamic behavior in the 1,4-cyclohexanedione−bromate−Ce(IV) system. Initial values: [CHD] = 0.09 mol/dm^3 and $[BrO_3^-] = 0.1$ mol/dm^3.

goes through one or more additional extrema after any initial excitable rebound and refractory period. Our simulations support the recent experimental results of Hamik and Steinbock,[9] who

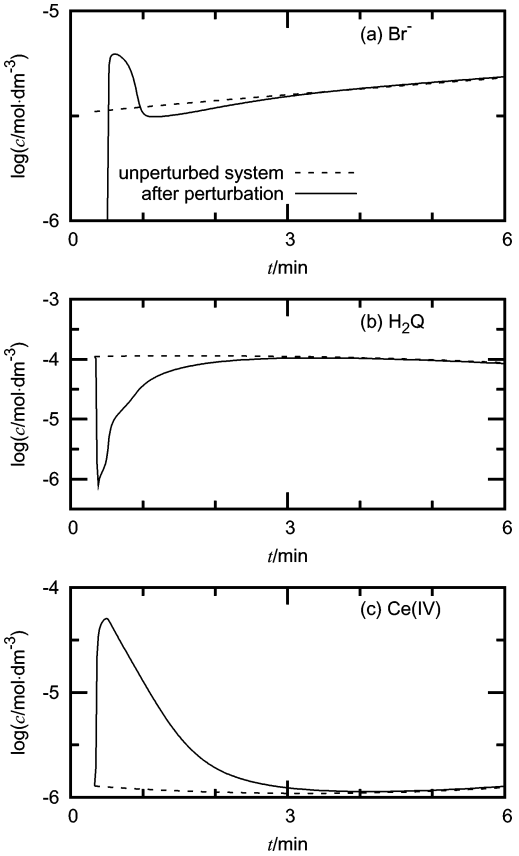

Figure 11. Nonmonotonic, nonoscillatory recovery in the 1,4-cyclohexanedione−bromate−Ce(IV) system. Dashed lines show behavior of the unperturbed system. Response of the system after perturbations in $[Br^-]$ (a), $[H_2Q]$ (b), and [Ce(IV)] (c). Initial values: $[BrO_3^-] = 0.1$ mol/dm^3; [CHD] = 0.09 mol/dm^3; [Ce(IV)] = 1.0×10^{-4} mol/dm^3; $[H_2SO_4] = 2.0$ mol/dm^3.

observed a monotonic recovery curve for the catalyst where the bromate−CHD−ferroin system shows anomalous dispersion.

As suggested in ref 7, the anomalous behavior appears to be due to the complexity caused by the dual control of the autocatalytic process by H_2Q and the catalyst. When the concentration of the catalyst is increased, control by the catalyst starts to prevail over control by H_2Q. As a result the nonmonotonic recovery disappears, the excitation threshold decreases, the shape of the excitation curve changes (Figure 12), and after perturbation the system stays in the excited state for a longer time.

Reduced Model. We have extracted a reduced model from the mechanism presented in Table 3. This skeleton model is shown in Table 5. Reaction R16′ in the reduced model is a combination of steps R16 and R17. We made the pool component approximation for CHD, BrCHD, BrO_3^-, and H^+. The other parameters in the reduced model are the total concentration of the catalyst $c_{tot} = ([Ox^{n+}] + [Red^{(n-1)+}])$ and the stoichiometric factor $f = \{[CHED] \times k_{10}\}/\{[BrCHD] \times k_9\}$, which gives the ratio of the production of bromide ions to that of H_2Q in the decomposition of BrCHD.[16] The parameter f is actually defined by choosing a value of the concentration of CHED. The rates of the reactions in the reduced model are summarized in Table 6. The simplified model contains 11 reactions (when ferroin is used, reaction R19 is also needed due to ferroin's relatively fast reaction with bromate compared to Ce(III), Mn(II), and $Ru(bipy)_3^{2+}$) and 5 variables. In the uncatalyzed bromate−CHD reaction, the stoichiometric factor f and the ratio of the concentration of bromate to that of BrCHD

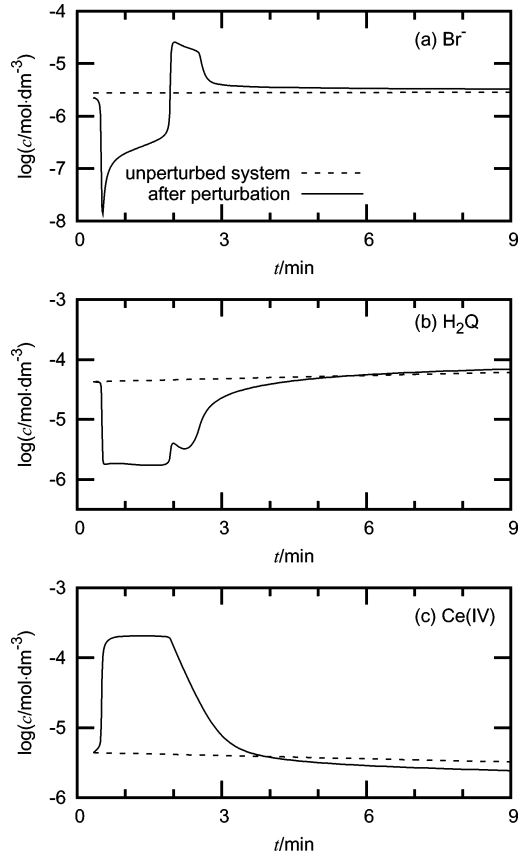

Figure 12. Excitability of the reduced state at higher concentration of Ce(IV). Response of the system after perturbations in $[Br^-]$ (a), $[H_2Q]$ (b), and [Ce(IV)] (c). Initial values: $[H_2SO_4] = 1.0$ mol/dm^3; $[BrO_3^-] = 0.1$ mol/dm^3; [CHD] = 0.09 mol/dm^3; [Ce(IV)] = 8.0×10^{-4} mol/dm^3.

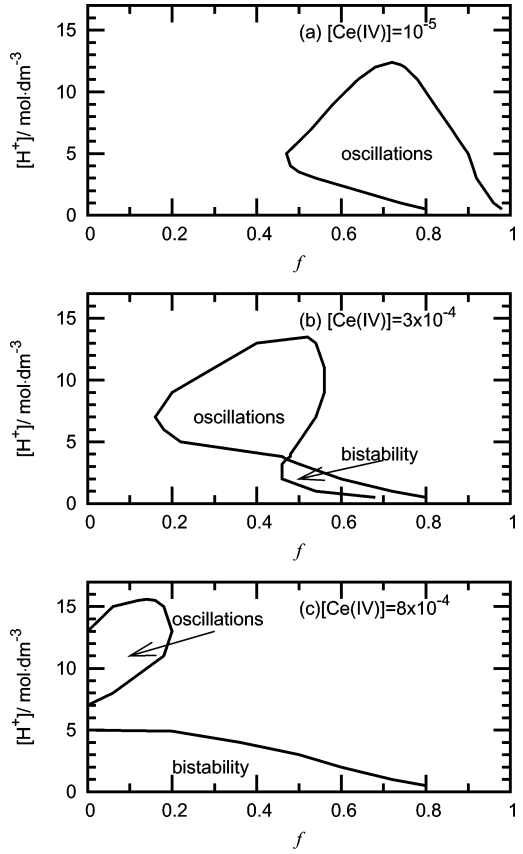

Figure 13. Phase diagram of the reduced model at several concentrations of Ce(IV). Initial values: $[BrO_3^-] = 0.08$ mol/dm^3; [CHD] = 0.08 mol/dm^3; (a) [Ce(IV)] = 1.0×10^{-5} mol/dm^3; (b) [Ce(IV)] = 3.0×10^{-4} mol/dm^3; (c) [Ce(IV)] = 8.0×10^{-4} mol/dm^3.

TABLE 5: Skeleton Model[a]

	reactions
R2	$\mathbf{Br^-} + \mathbf{HBrO_2} + H^+ \rightarrow 2HOBr$
R3	$\mathbf{Br^-} + BrO_3^- + 2H^+ \rightarrow \mathbf{HBrO_2} + 2HOBr$
R4	$\mathbf{2HBrO_2} \rightarrow BrO_3^- + HOBr + H^+$
R5	$\mathbf{HBrO_2} + BrO_3^- + H^+ \rightleftharpoons \mathbf{2BrO_2^\bullet} + H_2O$
R6a	$\mathbf{H_2Q} + \mathbf{2BrO_2^\bullet} \rightarrow \mathbf{2HBrO_2} + Q$
R6b	$Red^{(n-1)+} + \mathbf{BrO_2^\bullet} + H^+ \rightleftharpoons \mathbf{Ox}^{n+} + \mathbf{HBrO_2}$
R9	$BrCHD \rightarrow f\mathbf{H_2Q} + \mathbf{Br^-} + H^+$
R13	$\mathbf{H_2Q} + BrO_3^- + H^+ \rightarrow \mathbf{HBrO_2} + Q + H_2O$
R16′	$\mathbf{2Ox}^{n+} + BrCHD \rightarrow \mathbf{H_2Q} + \mathbf{Br^-} + 2Red^{(n-1)+} + ...$

[a] Variables are Br^-, $HBrO_2$, $BrO_2^\bullet$, H_2Q, and Ox^{n+}. The BrO_3^-, BrCHD, and H^+ are pool (constant concentration) components.

TABLE 6: Reaction Rates for a Skeleton Model

	rates
R2	$k_2 \times [Br^-] \times [HBrO_2] \times [H^+]$
R3	$k_3 \times [Br^-] \times [BrO_3^-] \times [H^+]^2$
R4	$k_{4b}k^f_{4a}/k^r_{4a} \times [H^+] \times [HBrO_2]^2$
R5^f	$k^f_{5a} \times [HBrO_2] \times [BrO_3^-] \times [H^+]$
R5^r	$k^r_{5a}\, k^r_{5b}/k^f_{5b} \times [BrO_2^\bullet]^2$
R6a	$k_{6a} \times [H_2Q] \times [BrO_2^\bullet]$
R6b^f	$k^f_{6b} \times (c_{tot} - [Ox^{n+}]) \times [BrO_2^\bullet] \times [H^+]$
R6b^r	$k^r_{6b} \times [Ox^{n+}] \times [HBrO_2]$
R9	$k_9 \times [BrCHD] \times [H^+]$
R13	$k_{13} \times [H_2Q] \times [BrO_3^-] \times [H^+]$
R16	$k_{16} \times [CHD] \times [Ox^{n+}]$

were found to be the key bifurcation parameters.[16] In the simulations of the detailed model and in the experiments both these quantities monotonically increase during the reaction. As shown here, the concentrations of acid and catalyst are also important parameters in determining the behavior of the bromate−CHD−catalyst systems.

On the phase diagram of the bromate−CHD−Ce(IV) system in the $[H^+]-f$ plane, one can follow the effect of increasing the catalyst concentration on the states. At low catalyst concentration the oscillatory domain is located at high values of f (∼0.7−1.0) (Figure 13a), as in the uncatalyzed case, where oscillations were found at f between 0.62 and 1.1.[16] At intermediate catalyst concentrations, oscillations and bistability were found in a typical cross-shaped diagram. The existence of bistability in the reduced model is an artifact caused by the pool component approximation. Of course, in the full batch model there is no bistability, but we have shown that at higher catalyst concentration the system stays for a significant time in the oxidized state after perturbation of the reduced state (Figure 12). In the closed bromate−CHD−ferroin system Chen[30] observed transient bistability and simulated it with an Oregonator-type model. At high catalyst concentration the oscillatory domain is shifted to low values of f (0−0.2), where we see "BZ-type" oscillations.

Changing the catalyst shifts the phase diagram as shown in Figure 14 but does not qualitatively change the behavior. At low acidity ($[H^+] = 1.0$ mol/dm^3]) the system shows uncatalyzed oscillations and bistability for all catalysts. The stability limit of the reduced state is the same ($f = 0.74$) for Ce(IV), Mn(II), and Ru(bipy)$_3^{2+}$ as for ferroin. The fast reaction of Ru(bypi)$_3^{3+}$ with CHD suppresses the oscillations at very low initial concentrations of the catalyst (∼6×10^{-6} mol/dm^3). In the case of ferroin the phase diagram is slightly different from the others because of the effect of reaction R19 which produces $HBrO_2$.

The five-variable model can be further reduced if a quasi-stationary approximation is applied to $BrO_2^\bullet$ and Br^-. The

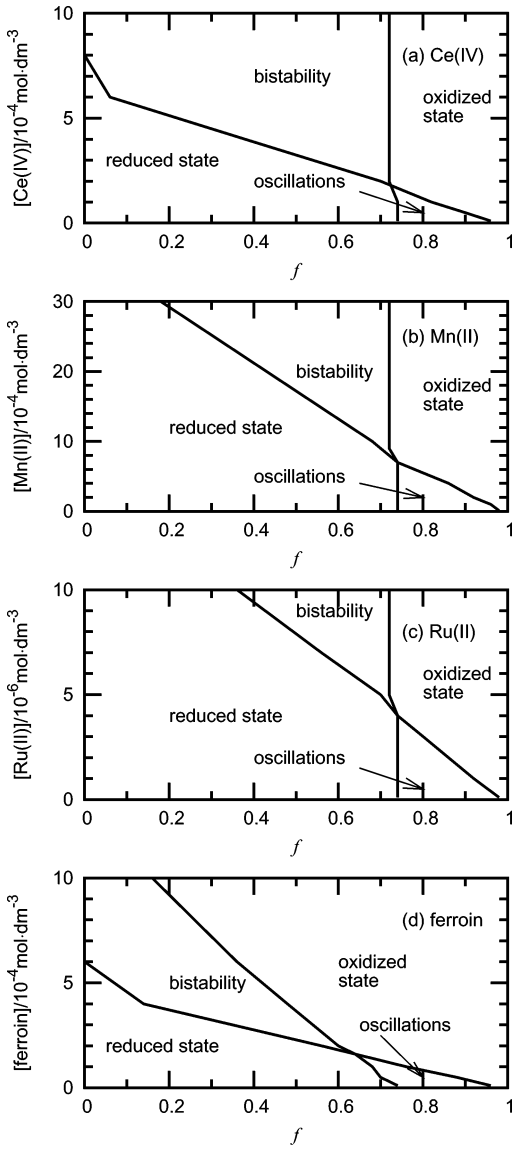

Figure 14. Phase diagram of the reduced model with different catalysts. Initial values: $[H^+] = 1.0$ mol/dm^3; $[BrO_3^-] = 0.08$ mol/dm^3; [CHD] $= 0.08$ mol/dm^3.

resulting three-variable model (the variables are $HBrO_2$, H_2Q, and Ox^{n+}) qualitatively reproduces all features of the five-variable scheme (oscillations, excitability, and bistability).

Conclusion

The oscillatory bromate−CHD system has been shown to exhibit rich dynamical behavior if a BZ catalyst (Ce(IV), Mn(III), Ru(bipy)$_3^{2+}$) is also present. These catalysts influence, proportionally to their concentrations, many parts of the oscillatory mechanism, which results in the appearance of a great variety of temporal and spatial phenomena in the bromate−CHD−catalyst batch systems. To explain some of these phenomena, we have augmented the mechanism suggested earlier for the bromate−CHD oscillator with reactions of the BZ catalyst. The catalysts effectively participate in both the positive and the negative feedback processes, i.e., they open a new autocatalytic pathway and enhance the production of the key intermediate H_2Q and the regeneration of the control intermediate Br^-. This extended version of the mechanism qualitatively describes all batch dynamics. The reduced model abstracted from the full mechanism allows us to derive bifurcation diagrams and to gain a qualitative understanding of the behavior of the system. For a description of the behavior of the catalyst-free bromate−CHD systems, a model with two variables ($HBrO_2$ and H_2Q) is sufficient. Introduction of the catalyst into the system and including a third (catalyst) variable in the model results in a significantly richer dynamics both in the experiments and in the simulations. Further improvement of the mechanism will require determination of the dependence of several rate constants on acidity and temperature. Work is in progress to measure these data and to incorporate them in our simulations. Modeling the effect of redox indicators such as diphenylamine or *p*-ethoxychrisoidine, which have lower redox potentials than the BZ catalysts but still influence the experimental behavior of the bromate−CHD reaction, is also a task for future research.

Acknowledgment. This work was financially supported by grants from the Hungarian Academy of Sciences (HAS) (OTKA T 043743 and F 034976), the Hungarian Ministry of Education (FKFP 0088/2001), the U.S. National Science Foundation (NSF), and a U.S.−Hungarian Cooperative Research Grant from NSF and HAS. The MULTIMRQ program was provided by the Femtochemistry Group of the Department of Physical Chemistry, Eötvös University.

References and Notes

(1) Kurin-Csörgei, K.; Zhabotinsky, A. M.; Orbán, M.; Epstein, I. R. *J. Phys. Chem.* **1996**, *100*, 5393.
(2) Winfree, A. T.; Caudle, S.; Chen, G.; McGuire, P.; Szilagyi, Z. *Chaos* **1996**, *6*, 617.
(3) Komlósi, A.; Nagy, I. P.; Bazsa, G. *J. Phys. Chem. A* **1998**, *102*, 9136.
(4) Fujieda, S.; Mori, Y.; Nkazawa, A.; Mogami, Y. *Adv. Space Res.* **2001**, *28*, 537.
(5) Davydov, V. A.; Manz, N.; Steinbock O.; Müller, S. C. *Europhys. Lett.* **2002**, *59*, 344.
(6) Manz, N.; Müller, S. C.; Steinbock, O. *J. Phys. Chem. A* **2000**, *104*, 5895.
(7) Hamik, C. T.; Manz, N.; Steinbock, O. *J. Phys. Chem. A* **2001**, *105*, 6144.
(8) Hamik, C. T.; Steinbock, O. *Phys. Rev. E* **2002**, *65*, 46224.
(9) Hamik, C. T.; Steinbock, O. *New J. Phys.* **2003**, *5*, 58.1
(10) Vanag, V. K.; Epstein, I. R. *Science* **2001**, *294*, 835.
(11) Vanag, V. K.; Epstein, I. R. *J. Phys. Chem.* **2002**, *106*, 11394.
(12) Yang, L.; Epstein, I. R. *J. Phys. Chem.* **2002**, *106*, 11676.
(13) Huh, D. S.; Choe, S. J.; Kim M. S. *React. Kinet. Catal. Lett.* **2001**, *74*, 11.
(14) Farage V. J.; Janjic D. *Chem. Phys. Lett.* **1982**, *102*, 301; **1982**, *93*, 621.
(15) Szalai, I.; Körös, E. *J. Phys. Chem. A* **1998**, *102*, 6892.
(16) Szalai, I.; Körös, E.; Györgyi, L. *J. Phys. Chem. A* **1999**, *103*, 243.
(17) Britton, M. *J. Phys. Chem. A* **2003**, *107*, 5033.
(18) Orbán, M.; Kurin-Csörgei, K.; Zhabotinsky, A. M.; Epstein, I. R. *J. Am. Chem. Soc.* **1998**, *120*, 1146.
(19) Szalai, I.; Kurin-Csörgei, K.; Orbán, M. *Phys. Chem. Chem. Phys.* **2002**, *4*, 1271
(20) Kéki, S.; Magyar, I.; Beck, M. T.; Gáspár, V. *J. Phys. Chem.* **1992**, *96*, 1725.
(21) Gao, Y.; Försterling, H. D. *J. Phys. Chem.* **1995**, *99*, 8638.
(22) Hindmarsh, A. C. *Livermore Solver for Ordinary Differential Equations*; Technical Report No. UCID-3001; Lawrence Livermore Laboratory: Livermore, CA, 1972.
(23) Wells, C. F.; Kuritsyn, L. V. *J. Chem. Soc. A* **1969**, 2575; **1969**, 2930; **1970**, 676.
(24) Mori, E.; Schreiber, I.; Ross, J. *J. Phys. Chem.* **1991**, *95*, 9395.
(25) Försterling, H. D.; Murányi, S.; Schreiber, H. *Z. Naturforsch.* **1989**, *44a*, 555.
(26) Försterling, H. D.; Varga, M. *J. Phys. Chem.* **1993**, *97*, 7932.
(27) Robertson, E. B.; Dunford, H. B. *J. Am. Chem. Soc.* **1964**, *86*, 5080.
(28) Zhang, Y.-X.; Field, R. J. *J. Phys. Chem.* **1990**, *94*, 7154.
(29) Elphick, C.; Meron, E.; Rinzel, J.; Spiegel, A. E. *J. Theor. Biol.* **1990**, *146*, 249.
(30) Chen, G. *Physica D* **2000**, *120*, 309.